Electronic Supplementary Material (ESI) for Journal of Materials Chemistry B.

Supplementary information

Self-recognizing and stimulus-responsive carrier-free metal-coordinated nanotheranostics for magnetic resonance/photoacoustic/fluorescence imaging-guided synergistic photo-chemotherapy

Li Tu[a], Zhongxiong Fan[a], Fukai Zhu[a], Qiang Zhang[a], Sen Zeng[a], Zhong Chen[d], Lei Ren[a], Zhenqing Hou[a,*], Shefang Ye[a,*], and Yang Li[b,c,*]

[a] Department of Biomaterials, College of Materials, Xiamen University, Xiamen 361005, China

[b] CAS Key Laboratory of Design and Assembly of Functional Nanostructures, and Fujian Provincial Key Laboratory of Nanomaterials, Fujian Institute of Research on the Structure of Matter, Chinese Academy of Sciences, Fuzhou 350002, China

[c] Department of Translational Medicine, Xiamen Institute of Rare Earth Materials, Chinese Academy of Sciences, Xiamen 361024, China

[d] School of Electronic Science and Engineering, Fujian Provincial Key Laboratory of Plasma and Magnetic Resonance, Xiamen University, Xiamen 361005, China

* Corresponding authors:

Prof. Zhenqing Hou, houzhenqing@xmu.edu.cn (Z. Hou)

Prof. Shefang Ye, yeshefang@xmu.edu.cn (S. Ye)

Prof. Yang Li, li.yang@fjirsm.ac.cn (Y. Li)

Experimental methods

Materials

All reagents are analytical grade and have not been further purified. Solutions were prepared using ultrapure water with the resistance of 18.5 MΩ.cm. Methotrexate (MTX) and folic acid (FA) were purchased from Bio Basic Inc. (Markham, Ontario, Canada). Indocyanine green (ICG) and 2, 7-dichlorofluorescein diacetate (DCFH-DA) were purchased from Sigma-Aldrich (USA). Iron(III) chloride hexahydrate ($FeCl_3 \cdot 6H_2O$) was purchased from Aladdin Reagent (Shanghai, China). Singlet oxygen sensor green (SOSG) was purchased from Thermo Fisher Scientific Inc. Anhydrous methanol, anhydrous ethanol, anhydrous diethyl ether, dimethyl sulfoxide (DMSO), and N, N-Dimethyl formamide (DMF) were supplied by Sinopharm Chemical Reagent Co., Ltd (Shanghai, China). Dulbecco's modified Eagle's medium (DMEM), Roswell Park Memorial Institute (RPMI) 1640, penicillin-streptomycin, fetal bovine serum (FBS), trypsin, 3-[4, 5-dimethylth-iazol-2-yl]-2, 5-

diphenyltetrazolium bromide (MTT), Dulbecco's phosphate-buffered saline (PBS), Hoechst 33258, Calcein-AM, and propidium iodide (PI) were purchased from Invitrogen (USA). Dihydroethidium (DHE), 4, 6-diamidino-2-phenylindole (DAPI), and Annexin V-FITC/PI staining kits were purchased from the Beyotime Institute of Biotechnology (Shanghai, China). HeLa, MCF-7, A549, and L02 cells were supplied by American Type Culture Collection (ATCC). BALB/c nude mice were provided by Xiamen University Laboratory Animal Center. All animal procedures were complied with the guidelines of the Xiamen University Institutional Animal Care and Use Committee.

Synthesis of MTX-Fe^{III} complex

In brief, $FeCl_3 \cdot 6H_2O$ (81.0 mg, 300 μM) was dissolved in 5 mL of anhydrous methanol. Then, 5 mL of methanol solution of $FeCl_3 \cdot 6H_2O$ was slowly added to MTX (22.7 mg, 50 μM) in DMF (0.5 mL) under agitation, and then stirred vigorously for 4 h at room temperature. Subsequently, the anhydrous methanol was removed through reduced pressure vacuum rotary evaporation. Finally, 10 mL of anhydrous diethyl ether was added to the obtained solution to facilitate the precipitation of the powder of MTX-Fe^{III} complex. The resulting precipitates were centrifugated (8000 rpm, 20 min), washed with ultrapure water and stored at -20 ^{o}C after freeze-drying for further use. In addition, other formulations with different molar ratios of MTX to Fe^{III} were prepared in the same procedure.

Preparation of ICG-MTX-Fe^{III}

ICG-MTX-Fe^{III} was prepared by anti-solvent method and co-assembly technique. Briefly, 4 mg of MTX-Fe^{III} was dissolved in 100 μL of DMSO, and 2 mg of ICG was dissolved in 50 μL of anhydrous ethanol, and then the two solutions were mixed. Subsequently, 6 mL of ultrapure water was injected dropwise into the mixed solution while stirring slightly. The reaction was stirred vigorously for another 6 h at room temperature. After that, the dispersion was dialyzed (MWCO: 1000 Da), centrifugated (16000 rpm, 20 min), washed with ultrapure water, and centrifuged again to remove the any residual organic solvents and free molecules. Finally, the obtained ICG-MTX-Fe^{III} was stored at -20 ^{o}C after freeze-drying. In addition, other formulations with different mass ratios of ICG to MTX-Fe^{III} were prepared in the same procedure.

Preparation of ICG-MTX

The preparation process of ICG-MTX was the same as that of ICG-MTX-Fe^{III}, except that MTX-Fe^{III} complex was replaced by MTX.

Characterization of ICG-MTX-Fe^{III}

The morphology of ICG-MTX-Fe^{III} with different mass ratios of ICG to MTX-Fe^{III} was observed by transmission electron microscopy (TEM, JEM 1400, JEOL, Japan) and atomic force microscopy (AFM, Multimode 8, Bruker, USA). Hydrodynamic diameter, zeta potential, and polydispersity index (PDI) were measured by dynamic light scattering (DLS) and electrophoretic light scattering (ELS) using the Malvern Nano-ZS (U. K.). Fourier transform infrared (FTIR) spectra were performed on the Avatar 370 infrared spectrometer (Nicolet, USA). Ultraviolet-

visible-near-infrared (UV-vis-NIR) absorption spectra were recorded with the Perkin Elmer Lambda 750 UV-vis-NIR spectrophotometer (USA) and fluorescence emission spectra were scanned with the FluoroMax-4 Spectrofluorometer (Horiba Jobin Yvon, France). TEM elemental mapping and energy dispersive spectrometer (EDS) detection were observed by transmission electron microscopy (TEM, Talos F200s, FEI, USA). X-ray photoelectron spectroscopy (XPS) analysis was carried out by X-ray chemical analysis electron spectra microprobe (Quantum 2000, Physical electronics, USA). The content of ferric ($Fe^{Ⅲ}$) ions in MTX-$Fe^{Ⅲ}$ complex or ICG-MTX-$Fe^{Ⅲ}$ was measured by inductively coupled plasma mass spectrometry (ICP-MS, 7500CE, Agilent Technologies, USA). The drug encapsulation efficiency (DEE) and loading capacity (DLC) were determined by dialysis (MWCO: 1000) and centrifugation (16000 rpm, 20 min). The free drugs were determined by UV-vis-NIR absorption spectra. In addition, DEE and DLC were calculated according to the following formulas:

$$DEE(\%) = \frac{m_T - m_U}{m_T} \times 100\% \qquad DLC(\%) = \frac{m_T - m_U}{m_S} \times 100\%$$

where m_T, m_U, and m_S are the total mass of feeding drug, the mass of the unencapsulated drug, and the mass of ICG-MTX-$Fe^{Ⅲ}$, respectively.

Stability evaluation

To evaluate *in vitro* spectral stability of ICG-MTX-$Fe^{Ⅲ}$ in PBS, the samples were stored in the dark at 25 ^{o}C for 120 h. At predetermined times, UV-vis-NIR

absorption and fluorescence spectra of ICG-MTX-Fe^{III} were measured. In addition, we used UV-vis-NIR spectrophotometer and spectrofluorometer to assess photodegradation and photobleaching of ICG-MTX-Fe^{III} and free ICG under continuous 5 min exposed to 808 nm laser (1 W/cm^2) irradiation. The stability of ICG-MTX-Fe^{III} in different physiological media (water, PBS, DMEM, and DMEM with 10% FBS) for different incubation time periods was evaluated by monitoring the hydrodynamic diameter and zeta potential using DLS and ELS.

***In vitro* photothermal effect**

200 μL of PBS, MTX-Fe^{III}, ICG, and ICG-MTX-Fe^{III} at different concentrations of ICG (5, 10, 15, 20, and 25 μg/mL) were added into EP tubes and irradiated by continuous 808 nm laser with different laser power intensities (0.5, 1.0, and 1.5 W/cm^2) for 5 min. Infrared thermograms and temperatures were recorded by thermal infrared imaging camera (FLIR A5, FLIR Systems, USA).

Photothermal conversion efficiency

To further study the photothermal performance of ICG-MTX-Fe^{III}, we calculated the photothermal conversion efficiency (η) using the following equation:

$$\eta = \frac{hS(T_{\max} - T_{surr}) - Q_0}{I(1-10^{-A_{808}})} \quad (1)$$

$$hS = \frac{m_d C_d}{\tau_s} \quad (2)$$

$$t = -\tau_s \ln(\frac{T - T_{surr}}{T_{\max} - T_{surr}}) \quad (3)$$

$$Q_0 = hS(T_{\max,water} - T_{surr}) \quad (4)$$

where h represents the heat transfer coefficient; S represents the surface area of sample container; T_{max} and T_{surr} represent the maximum temperature and the room temperature, respectively; Q_0 represents the heat dissipation of the solvent; I represents the laser power at 808 nm; A_{808} represents the absorbance of ICG-MTX-$Fe^{Ⅲ}$ at 808nm. The value of hS was calculated by eq (2). Where τ_s represents the characteristic thermal time constant; m_d and C_d represent the mass of solution (g) and heat capacity (4.2 J/g). The value of τ_s was calculated by eq (3). Where t and T represent the cooling time and the corresponding temperature, respectively. Q_0 was calculated by using the following eq (4).

***In vitro* singlet oxygen ($^1O_2$) generation**

The generation of $^1O_2$ was measured by a commercial assay kit based on SOSG. PBS, MTX-$Fe^{Ⅲ}$, ICG (15 μg/mL), and ICG-MTX-$Fe^{Ⅲ}$ containing different concentrations of ICG (5, 10, 15, 20, and 25 μg/mL) were mixed with 10 μM of SOSG, respectively. After irradiation with 808 nm laser (1 W/cm^2) for 5 min, the fluorescence intensity of these samples was detected by fluorescence spectrometer at excitation wavelength of 504 nm and emission wavelength of 525 nm.

***In vitro* magnetic resonance (MR) imaging**

ICG-MTX-$Fe^{Ⅲ}$ with different $Fe^{Ⅲ}$ ion concentrations (0, 0.0125, 0.025, 0.05, 0.1,

and 0.2 mM) was dispersed in the hot agarose liquid (0.9 w/v%), and T_1 relaxivity was detected by 7.0 T MR scanner (Bruker, Germany). T_1 relaxation rates under 7.0 T field were plotted against the $Fe^{Ⅲ}$ ion contents. The relaxivity of ICG-MTX-$Fe^{Ⅲ}$ was finally acquired by linear fitting analysis. MTX-$Fe^{Ⅲ}$ complex was used as a control.

***In vitro* photoacoustic (PA) imaging**

PBS, MTX-$Fe^{Ⅲ}$, ICG (15 μg/mL), and ICG-MTX-$Fe^{Ⅲ}$ containing different concentrations of ICG (5, 10, 15, 20, and 25 μg/mL) were added into EP tubes and immersed in water tank. The PA signals of these samples were captured at 808 nm by PA imaging system (Vevo 2100, Visual Sonics, Canada).

***In vitro* disassembly and drug release**

In vitro release profiles of both ICG and MTX from ICG-MTX-$Fe^{Ⅲ}$ were determined by adding 3 mL solution of ICG-MTX-$Fe^{Ⅲ}$ (1 mg/mL) into dialysis bags (MWCO: 3500 Da), which were immersed into 47 mL of PBS at different pH conditions (7.4, 6.5, and 5.0). The release experiment was performed with/without 808 nm laser (1 W/cm^2) irradiation for 5 min at initial time of experiment. At 37 ^{o}C, the test bags were gently shaken in the rotary shaker at 100 rpm. At predetermined time intervals, the dialysate was withdrawn followed by replacing with the equal volume of fresh PBS to continue study. The release amount of MTX and ICG in the dialysate was measured by UV-vis-NIR absorption spectra. In addition, the morphologic changes of ICG-MTX-$Fe^{Ⅲ}$ at different pH conditions with/without 808

nm laser irradiation were analyzed by TEM.

Cell culture

HeLa (cervical carcinoma) and MCF-7 cells (breast carcinoma) were chosen for the following experiments due to their high-levels of folate receptor expression. A549 cells (lung carcinoma) were chosen as a comparison due to their low-levels of folate receptor expression. L02 cells (normal hepatocyte) were chosen as a blank control. The cells were cultured in RPMI 1640 medium or DMEM medium containing 10% FBS and 1% penicillin/streptomycin in a water-jacketed CO_2 incubator (Thermo Fisher Scientific Inc., USA) with 5% CO_2 at 37 ^oC.

***In vitro* cellular uptake**

Cellular uptake was evaluated using HeLa cells, A549 cells, and L02 cells. Three kinds of cell lines were seeded in 6-well plates with 2×10^5 cells per well, and cultured for 24 h until fully attached. Afterward, the cells were treated with ICG, ICG/MTX-$Fe^{Ⅲ}$ mixture, and ICG-MTX-$Fe^{Ⅲ}$ at equivalent concentration of ICG (10 μg/mL). After incubation for specific time periods at 37 ^oC, the cells were washed thrice with PBS, stained with Hoechst 33258 for 15 min, and then fixed with 4% paraformaldehyde for 20 min. Finally, confocal laser scanning microscope (CLSM, Leica TCS SP5, USA) was applied to observe cellular uptake. In addition, to investigate the competitive inhibition effect, the cells were preincubated in medium supplemented with excessive free FA for 2 h before adding drug formulations.

For further quantification, the cells (1×10^5 cells per well) were seeded in 12-well

plates. After culture for 24 h, the cells were treated with ICG, ICG/MTX-Fe^{III} mixture, and ICG-MTX-Fe^{III} at equivalent concentration of ICG (5 μg/mL) for specific incubation time periods with/without pretreatment of free FA. Then, the cells were trypsinized, washed with PBS, and resuspended in PBS. The fluorescence intensity of intracellular ICG was recorded by FACSCalibur flow cytometer (Becton Dickinson, USA) and the data were analyzed by CellQuest/FlowJo software.

Detection of intracellular reactive oxygen species (ROS)

Intracellular $^1O_2$ generation was tested by DCFH-DA, which could be ingested by cells and converted into fluorescent DCF in the presence of ROS, showing strong fluorescence. Specifically, HeLa cells were seeded in 6-well plates with 2×10^5 cells per well, and cultured for 24 h until fully attached. Then, the cells were washed with PBS and incubated with ICG, ICG/MTX-Fe^{III} mixture or ICG-MTX-Fe^{III} at the equivalent concentration of ICG (5 μg/mL) for 8 h. Afterwards, the cells were incubated with DCFH-DA (10 μM) for another 30 min. After washing for three times, the cells were exposed to 808 nm laser (0.5 W/cm^2) for 5 min. The generation of $^1O_2$ was evaluated by CLSM and FACSCalibur flow cytometer.

***In vitro* cytotoxicity**

Cytotoxicity was assessed by the MTT assay according to the manufacturer's suggested procedures. HeLa or MCF-7 cells were seeded in 96-well plates at the density of 1×10^4 cells per well. After culture for 24 h, the DMEM with various concentrations of ICG, MTX, MTX-Fe^{III} complex, and ICG-MTX-Fe^{III} were added

into each well. The MTX concentrations (1, 2, 5, 10, 20, and 40 μg/mL) of ICG-MTX-$Fe^{Ⅲ}$ were equivalent to the corresponding concentrations of MTX. And the ICG concentrations (0.5, 1, 2.5, 5, 10, and 20 μg/mL) of ICG-MTX-$Fe^{Ⅲ}$ were equivalent to the corresponding concentrations of ICG. After incubation for 8 h, the cells were irradiated with 808 nm laser (1 W/cm^2) for 5 min. Control cells were identically treated but not received laser irradiation. After incubation of cells with different drug formulations for another 16 h, the culture medium was removed, the culture medium containing 10 μL of MTT solution (5 M, PBS as the solvent, pH 7.4) was added to each well, and the cells were treated for another 4 h. Then, the MTT solution was removed and DMSO (150 μL) was added to each well. These plates were agitated for 20 min to adequately dissolve the formazan crystals. The absorbance was measured at 490 nm by microplate reader (TECAN, Infinite M200 PRO, Switzerland). Cell viability (%) was calculated as (OD of test group)/(OD of control group) × 100%, in which OD is optical density. In addition, to evaluate the competitive inhibition effect, the cells were pretreated in medium supplemented with excessive free FA for 2 h before adding the drug formulations.

Meanwhile, living and dead cells were stained with Calcein-AM and PI, respectively. Cell culture medium containing ICG, MTX, MTX-$Fe^{Ⅲ}$, and ICG-MTX-$Fe^{Ⅲ}$ were used for culturing HeLa cells in 6-well plates with 5×10^5 cells per well for 8 h, the concentration of MTX was 40 μg/mL. These cells were irradiated with/without 808 nm laser (1 W/cm^2) for 5 min and incubated for another 16 h. According to the manufacturer's suggested protocol, a live/dead staining kit was used

to differentiate the living cells and dead cells by fluorescence microscope (Leica Microsystems, Germany).

In vitro synergistic effect

The combination index (CI) of ICG-MTX-Fe^{III} was calculated according to the following formula: CI_x = (IC_x of MTX in ICG-MTX-Fe^{III}/IC_x of free MTX) + (IC_x of ICG in ICG-MTX-Fe^{III} with laser irradiation/IC_x of free ICG with laser irradiation).

In vitro apoptosis assay

HeLa cells were seeded in 12-well plates with 2×10^5 cells per well, and cultured for 24 h until all cells were fully attached. The cells were treated with ICG (10 μg/mL), MTX (20 μg/mL), MTX-Fe^{III} (20 μg/mL), and ICG-MTX-Fe^{III} (containing 20 μg/mL of MTX) for 8 h, then applied for 808 nm laser (1 W/cm^2) irradiation for 5 min. Control cells were identically treated but not received laser irradiation. 24 h later, all cells were harvested and collected in EP tubes, washed twice (1000 rpm, 3 min) with PBS, and then suspended in 195 μL of binding buffer. Then, 5 μL of Annexin V-FITC was added to each tube and incubated for 10 min in dark at 25 ^oC. After gentle vortex and centrifugation (1000 rpm, 3 min), the cells were resuspended in 190 μL of binding buffer and 10 μL of PI was added to each tube. Finally, the cell apoptosis levels were determined by FACSCalibur flow cytometer.

In vitro hemolysis analysis

The hemolysis assay was employed to evaluate the blood compatibility. The

fresh rabbit blood containing 0.1% heparin sodium was centrifuged at 3000 rpm for 10 min and washed three times with PBS. The washed red blood cells were suspended in PBS. ICG, MTX, MTX-$Fe^{Ⅲ}$, ICG/MTX-$Fe^{Ⅲ}$ mixture, and ICG-MTX-$Fe^{Ⅲ}$ were added into the 2% red blood cells. After incubation at 37 ^{o}C for 12 h, the samples were centrifuged and the absorbance values of the supernatant at 541 nm were determined by microplate reader. PBS and ultrapure water were used as negative and positive control, respectively. The hemolysis percent of RBCs was determined after incubation according to the following formula: hemolysis percentage (%) = (A_{sample} – A_{PBS})/(A_{water} – A_{PBS}) × 100%, where A_{sample}, A_{PBS}, and A_{water} are the 541 nm absorbance values of the sample groups, the PBS group, and the ultrapure water group, respectively.

Animals

Animal experiments were carried out according to the guidelines and policies approved by the Institutional Animal Care and Use Committee of Xiamen University. BALB/c nude mice (female, 7-8 week) were provided from Experimental Animal Laboratory of Cancer Research Center of Xiamen University.

***In vivo* fluorescence (FL) imaging**

HeLa cells (5×10^6 cells in 100μL of PBS) were subcutaneously injected into the right leg of each nude mouse to establish the HeLa tumor-bearing mouse model. When the tumors grew up to an average volume of about 80 mm^3, the mice were randomly divided into two groups (n = 4) and intravenously injected with ICG and

ICG-MTX-Fe^{Ⅲ}, respectively. ICG dosage in mice was 2 mg/kg. At 0, 1, 2, 4, 12, 24, and 36 h after intravenous injection, FL imaging was recorded by IVIS Lumina imaging system (Caliper Life Sciences, USA). In addition, the FL intensity was semi-quantitatively analyzed by Living Image Software.

***In vivo* PA imaging**

Vevo 2100 Imaging System was used to perform the *in vivo* PA imaging experiment when the tumor volume reached around 100 mm^3. HeLa tumor-bearing nude mice were divided into two groups (n = 4) and intravenously injected with ICG or ICG-MTX-Fe^{Ⅲ}. ICG dosage in mice was 2 mg/kg. PA imaging of tumors were recorded with the excitation wavelength of 808 nm at certain time intervals.

***In vivo* MR imaging**

MR imaging was performed when the tumor volume reached around 100 mm^3. HeLa tumor-bearing nude mice were assigned into two groups (n = 4) and intravenously injected with MTX-Fe^{Ⅲ} or ICG-MTX-Fe^{Ⅲ}. MTX-Fe^{Ⅲ} dosage in mice was 6.66 mg/kg. Subsequently, the treated mice were monitored by Bruker Biospec 7.0 T MR scanner at predetermined times.

***In vivo* photothermal therapy (PTT)**

HeLa tumors were generated by the same procedure as previously described. When the tumor volume reached about 100 mm^3, the mice were divided into three groups (n = 4) by random and injected with PBS, ICG (2 mg/kg), and ICG-MTX-Fe^{Ⅲ}

(equivalent to 2 mg/kg of ICG) *via* caudal veins. During the 10-min irradiation with 808 nm laser (1 W/cm^2), the real-time tumor temperature of mice was recorded by FLIR A5 thermal imaging camera at 24 h post-injection.

In vivo photodynamic therapy (PDT)

To evaluate the photodynamic effect of ICG-MTX-Fe^{III} *in vivo*, another batch of HeLa tumor-bearing nude mice models were established. When the tumor volume grew up to about 100 mm^3 in volume, various formulations (PBS, ICG, and ICG-MTX-Fe^{III}) at equivalent dosage of ICG (2 mg/kg) were injected into the mice *via* caudal veins. At 24 h post-injection, the tumor areas of mice were exposed to 808 nm laser (1 W/cm^2) irradiation for 10 min. Subsequently, the tumors were developed into frozen slices to visualize the ROS fluorescence distribution. ROS distribution was monitored by fluorescence microscopy using DHE as the indicator. Sections of whole tumor were stained using DAPI to label all nuclei of tumor cells.

In vivo pharmacokinetics

When the average tumor volume was about 80 mm^3, HeLa tumor-bearing nude mice were randomly divided into two groups (n = 4) and intravenously injected with ICG (2 mg/kg) and ICG-MTX-Fe^{III} (equivalent to 2 mg/kg of ICG), respectively. Blood samples were taken from the mice's orbits at different predetermined time points, and then the concentrations of ICG were determined by fluorescence spectrometer.

In vivo biodistribution

HeLa tumor-bearing nude mice injected with ICG-MTX-Fe^{III} (equivalent to 2 mg/kg of ICG) *via* caudal veins were sacrificed after 24, 48, and 72 h, respectively. Major organs and tumors were collected and homogenized in PBS. Subsequently, the homogenates were centrifuged at 3000 rpm for 10 min and the supernatants were harvested to determine the mass of ICG in heart, liver, spleen, lung, kidney, and tumors using fluorescence spectrometer, respectively.

***In vivo* antitumor effect**

The tumor models were established by inoculated HeLa cells (5× 10^6 cells per tumor) into right leg areas of the nude mice. After the tumors reached about 100 mm^3, the mice were divided into seven groups (n = 4): PBS-treated group, Laser-treated group, ICG-treated group, ICG/Laser-treated group, MTX-Fe^{III}-treated group, ICG-MTX-Fe^{III}-treated group, and ICG-MTX-Fe^{III}/Laser-treated group. These materials were injected into the mice *via* caudal veins. The dose of MTX-Fe^{III} and ICG was ~4 mg/kg and ~2 mg/kg, respectively. And the dose of ICG-MTX-Fe^{III} was ~6 mg/kg (~4 mg/kg of MTX-Fe^{III} and ~2 mg/kg of ICG). The tumor areas of mice in groups (b), (d), and (g) were irradiated with 808 nm laser (1 W/cm^2) for 10 min at 24 h post-administration *via* caudal veins of the mice. Afterwards, the tumor volume and body weight were recorded every day for two weeks. The following formula was applied to calculate tumor volume: $V = A \times B^2/2$, where A is the largest diameter and B is the smallest diameter.

The mice were sacrificed after 14 days, the tumor tissues were isolated for

excised volume and weight measurements. Tumor inhibition ratio was calculated according to the following equation:

$$\text{Tumor inhibition ratio (\%)} = \frac{W_c - W_t}{W_c} \times 100\%$$

where W_c is the average tumor weight of control group, while W_t is the average tumor weight of treatment group.

Histological assessment

The tumor tissues of mice in each group were collected after 7 days of treatment, and the main organs of mice in experimental and control groups were harvested at the end of the experiment. For histological analysis, the major organs and tumors were fixed in 4% paraformaldehyde, embedded in paraffin, cut into slices, and stained with hematoxylin and eosin. Then, these sections were observed under optical microscope (BX53, Olympus, Japan).

Statistical analysis

Data statistics were analyzed by calculating the *t*-test between two groups, and One-way ANOVA analysis of variations for multiple groups. Unless otherwise noted, all results were expressed as the mean ± standard deviation (SD). A value of $p < 0.05$ was indicated by a single asterisk (*) and was considered statistically significant.

Table S1 The encapsulation efficiency of ICG and MTX in ICG-MTX-Fe^{III} (n = 4).

1: Mass	2 ratio	of	ICG	31 Drug	.5 loadi	ng	±	1. capa	·	62 Drug	.3 loadi	ng	±	2. capa

Table S2 The loading capacity of ICG and MTX in ICG-MTX-Fe^{III} with an optimized mass ratio of ICG to MTX-Fe^{III} (1: 2) (n = 4).

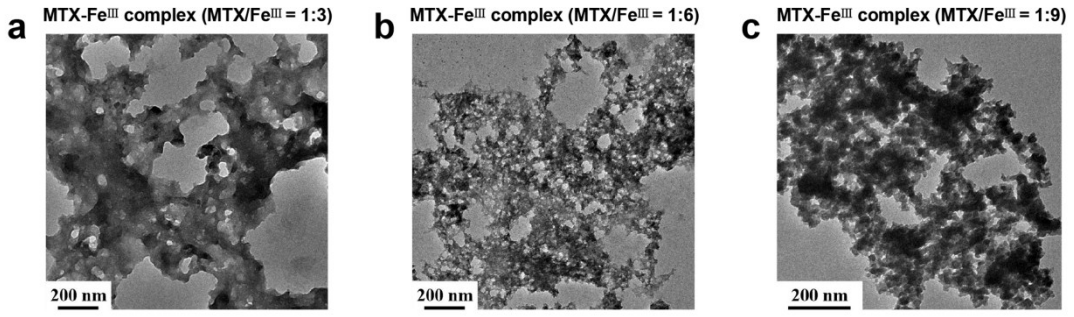

Fig. S1 TEM micrographs of MTX-Fe^{III} complex at MTX/Fe^{III} molar ratios of (a) 1: 3, (b) 1: 6, and (c) 1: 9.

Through numerous attempts to test a series of molar ratios of MTX/Fe^{III} by using TEM, we found that the morphology of MTX-Fe^{III} complex was irregular, and that the MTX-Fe^{III} intermediate could not be self-assembled to form monodisperse nanoparticals.

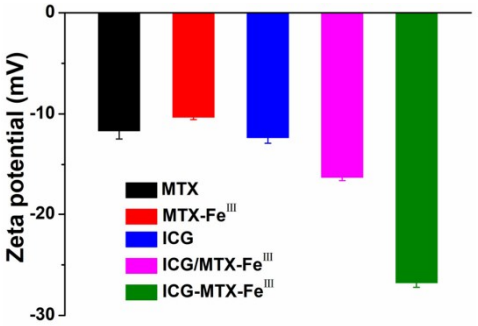

Fig. S2 Zeta potential of MTX, MTX-Fe^{III}, ICG, ICG/MTX-Fe^{III} mixture (physical mixture of ICG and MTX-Fe^{III}, ICG/MTX-Fe^{III} = 1: 2), and ICG-MTX-Fe^{III}. Error bars represent mean ± SD (n = 4).

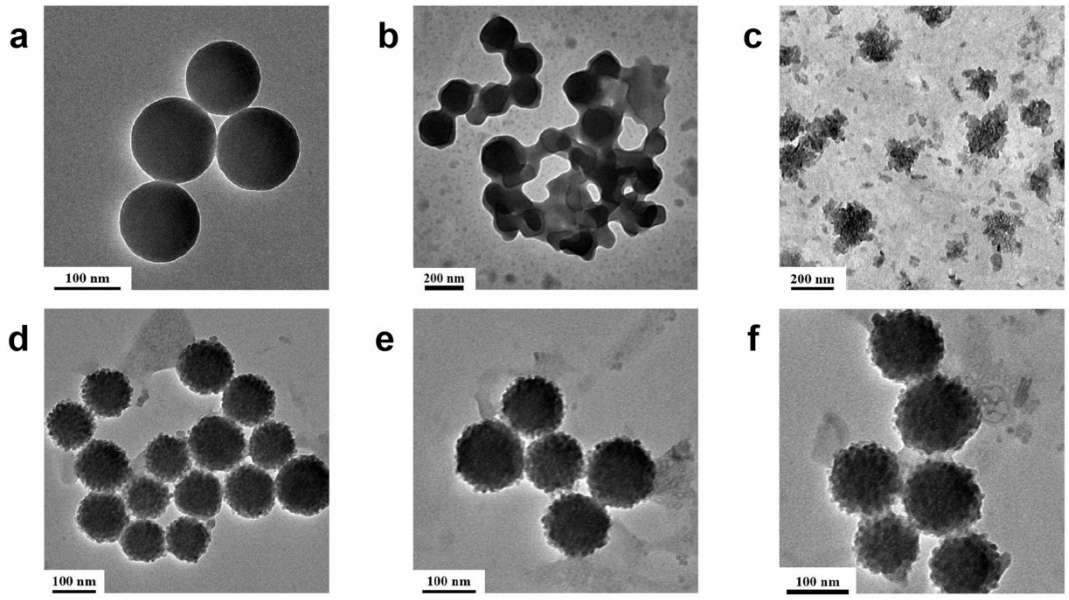

Fig. S3 TEM micrographs of ICG-MTX (without metal coordination, ICG/MTX = 1: 2) (a) before and (b) after dilution. (c) TEM micrograph of ICG-MTX in PBS after kept for 24 h. TEM micrographs of ICG-MTX-Fe^{III} (ICG/MTX-Fe^{III} = 1: 2) (d) before

and (e) after dilution. (f) TEM micrograph of ICG-MTX-Fe^{III} in PBS after kept for 24 h. The samples were diluted 5×.

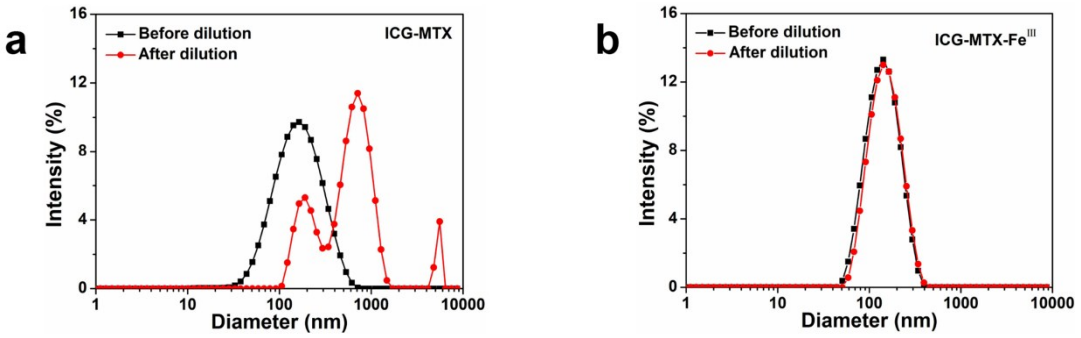

Fig. S4 Hydrodynamic diameter distribution of (a) ICG-MTX and (b) ICG-MTX-Fe^{III} before and after dilution.

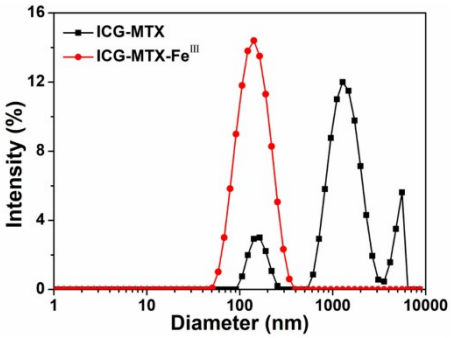

Fig. S5 Hydrodynamic diameter distribution of ICG-MTX and ICG-MTX-Fe^{III} in PBS after kept for 24 h.

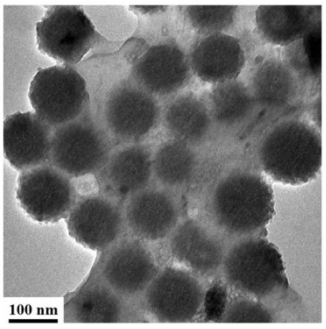

Fig. S6 TEM micrograph of ICG-MTX-Fe^{III} in PBS after kept for a week.

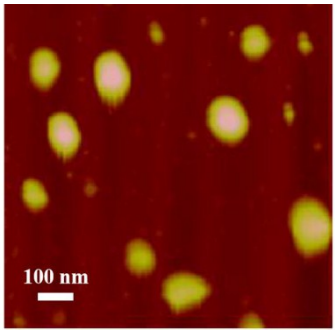

Fig. S7 AFM micrograph of ICG-MTX-Fe^{III}.

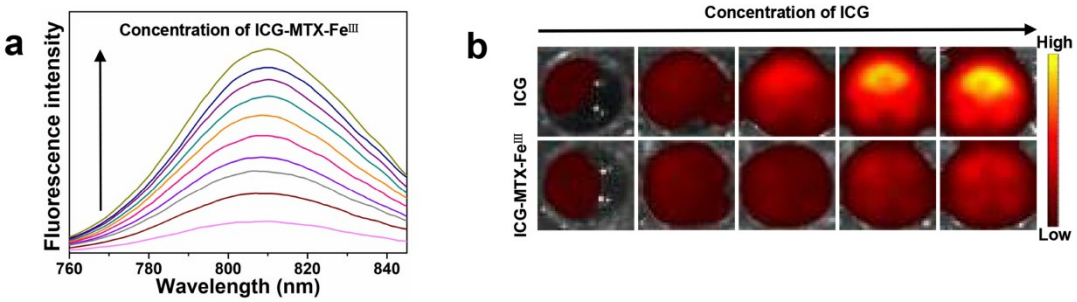

Fig. S8 (a) Fluorescence spectra and (b) fluorescence images of ICG-MTX-Fe^{III}

containing different concentrations of ICG.

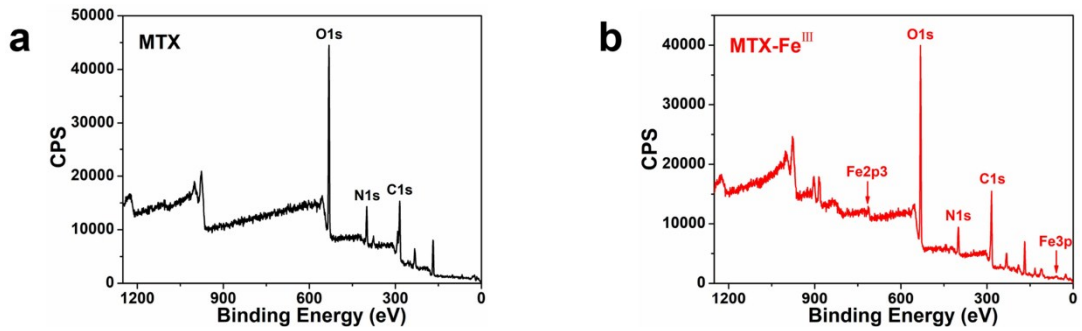

Fig. S9 XPS analysis of (a) MTX and (b) MTX-Fe^{III} complex.

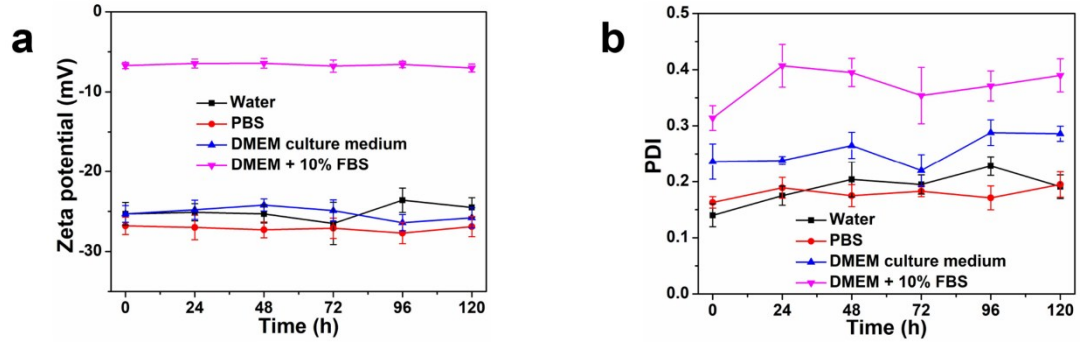

Fig. S10 Changes of (a) zeta potential and (b) PDI of ICG-MTX-Fe^{III} in different media during 120 h. Error bars represent mean ± SD (n = 4).

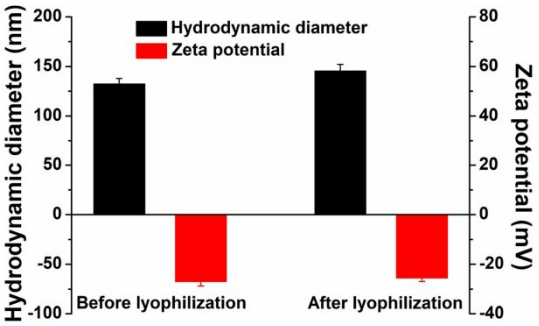

Fig. S11 Changes of hydrodynamic diameter and zeta potential of ICG-MTX-Fe^{III} before and after lyophilization. Error bars represent mean ± SD (n = 4).

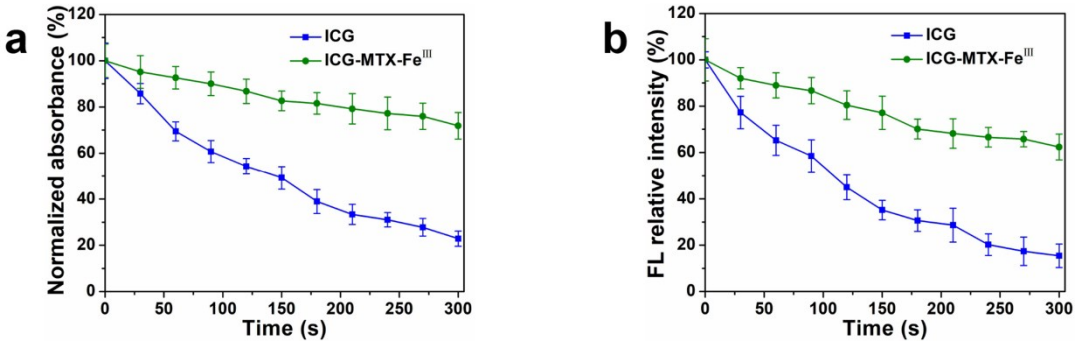

Fig. S12 Time-dependent variations of (a) absorbance and (b) fluorescence of ICG and ICG-MTX-Fe^{III} under 808 nm laser irradiation. Error bars represent mean ± SD (n = 4).

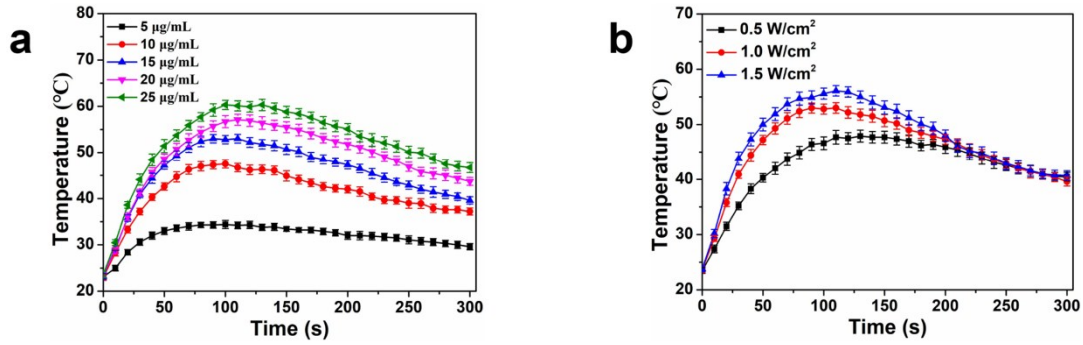

Fig. S13 Photothermal heating curves of ICG at different (a) concentrations and (b) laser power intensities. Error bars represent mean ± SD (n = 4).

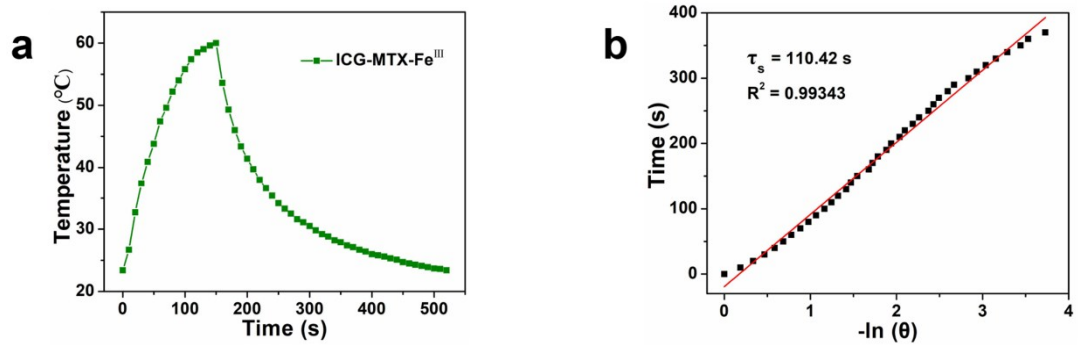

Fig. S14 (a) Photothermal heating and cooling curves of ICG-MTX-Fe$^{\text{Ⅲ}}$. (b) Linear fitting between the cooling time data versus -ln (θ).

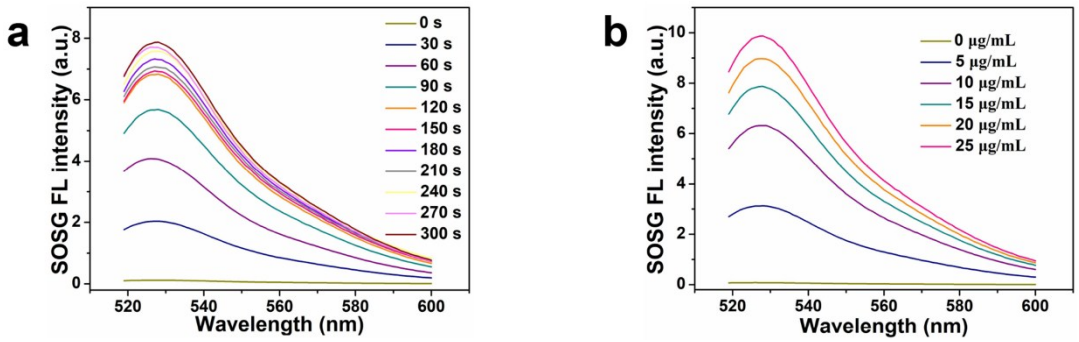

Fig. S15 SOSG fluorescence spectra of ICG-MTX-Fe^{III} at different (a) laser irradiation time and (b) concentrations of ICG.

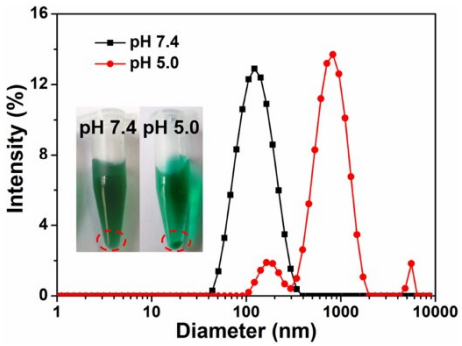

Fig. S16 pH-responsive disassembly of ICG-MTX-Fe^{III}.

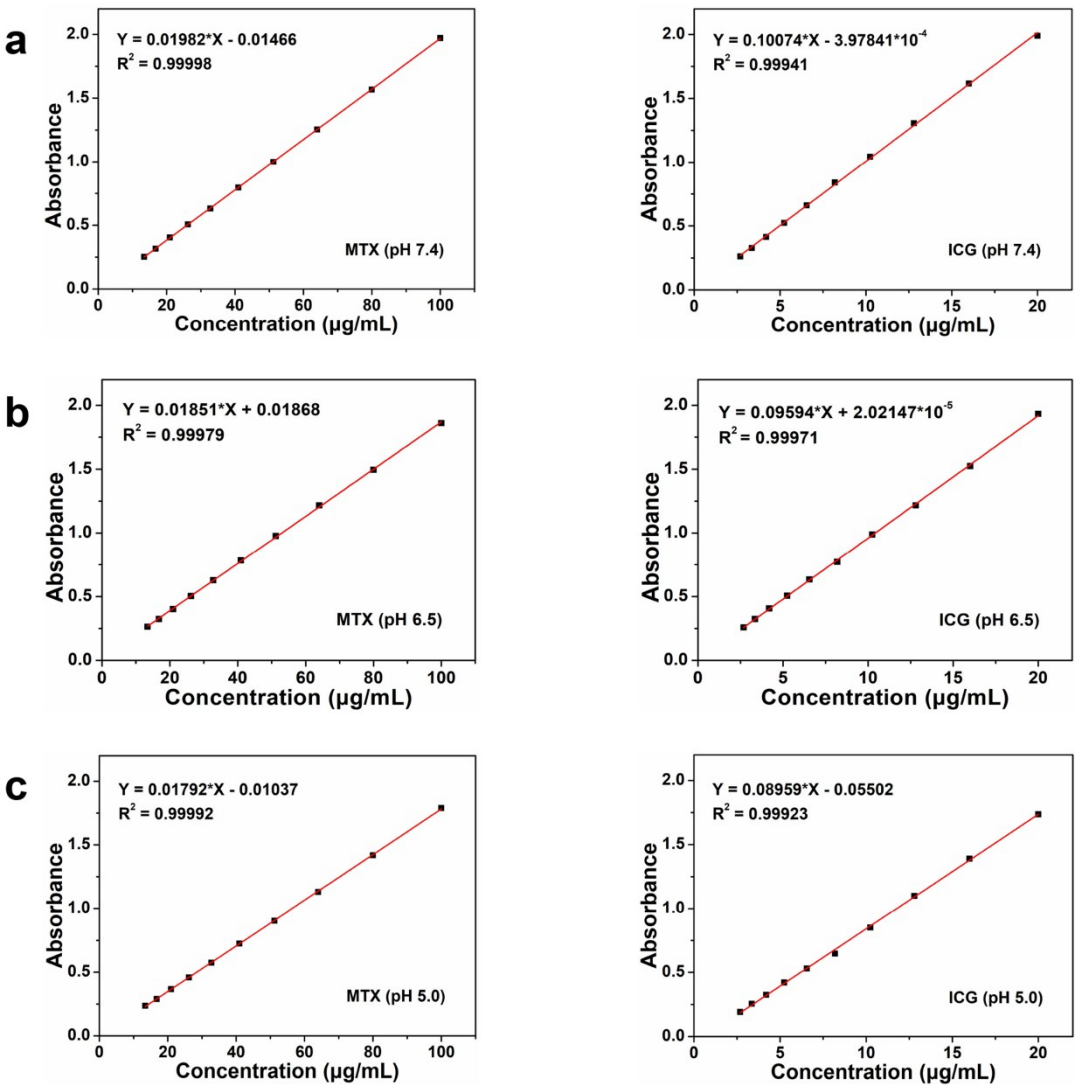

Fig. S17 The standard curves of MTX and ICG at different pH conditions (7.4, 6.5, and 5.0).

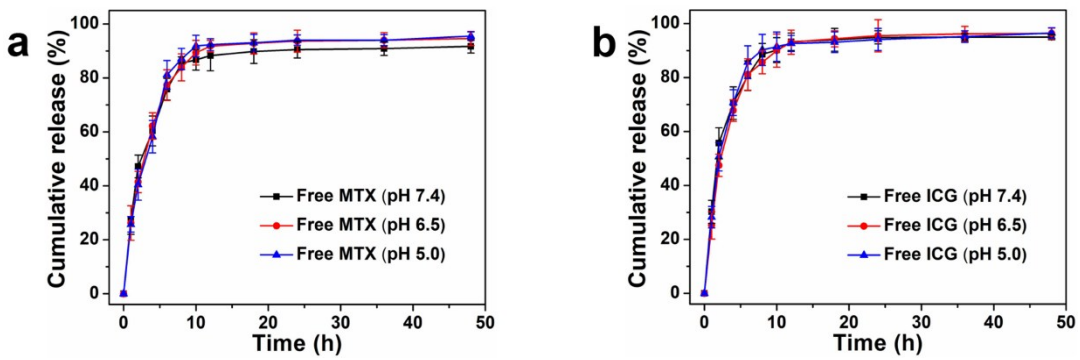

Fig. S18 Cumulative release curves of (a) free MTX and (b) free ICG at different pH conditions (7.4, 6.5, and 5.0). Error bars represent mean ± SD (n = 4).

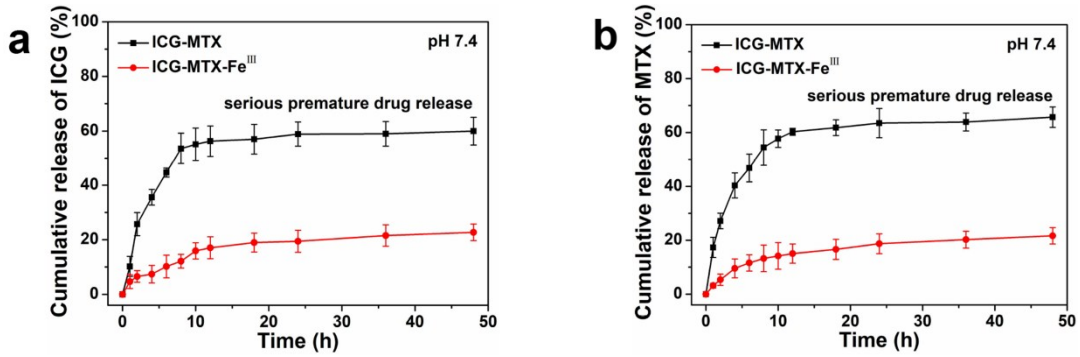

Fig. S19 Cumulative release curves of (a) ICG and (b) MTX from ICG-MTX and ICG-MTX-Fe^{III} at pH 7.4. Error bars represent mean ± SD (n = 4).

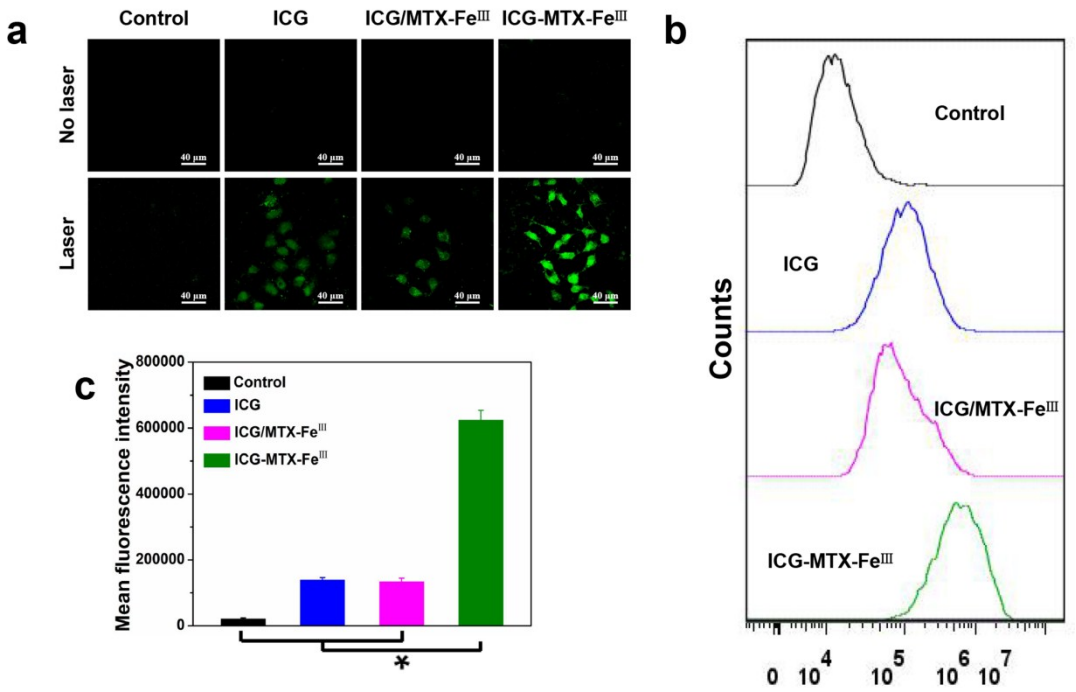

Fig. S20 (a) CLSM images and (b, c) flow cytometry analysis of DCFH-DA-stained HeLa cells after incubation with ICG, ICG/MTX-Fe^{III} mixture, and ICG-MTX-Fe^{III} for 8 h with/without laser irradiation. Error bars represent mean ± SD (n = 4); *P < 0.05.

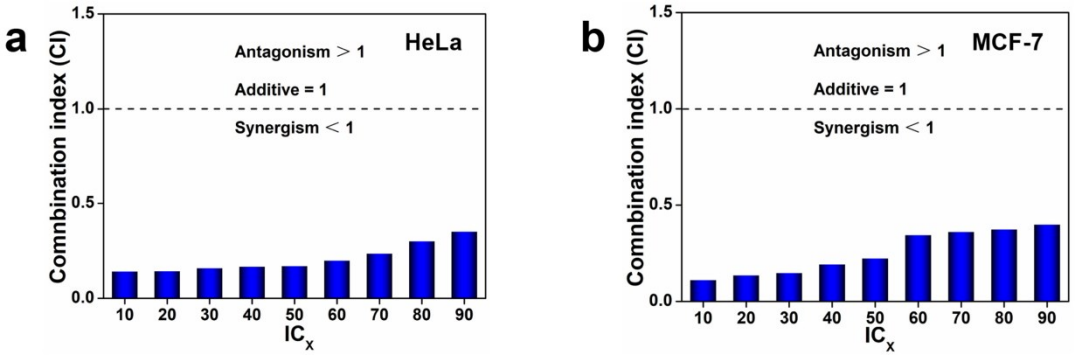

Fig. S21 Combination index (CI) values of (a) HeLa and (b) MCF-7 cells incubated with ICG-MTX-Fe^{III} under laser irradiation. CI value < 1 indicates synergism, CI

value = 1 indicates additivity, and CI value > 1 indicates antagonism.

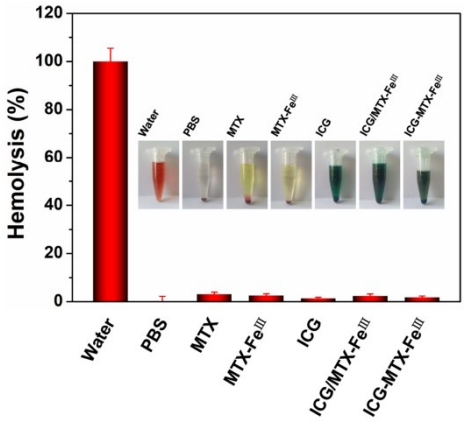

Fig. S22 Hemolysis test of MTX, MTX-Fe^{III}, ICG, ICG/MTX-Fe^{III} mixture, and ICG-MTX-Fe^{III} on RBCs. Error bars represent mean ± SD (n = 4).

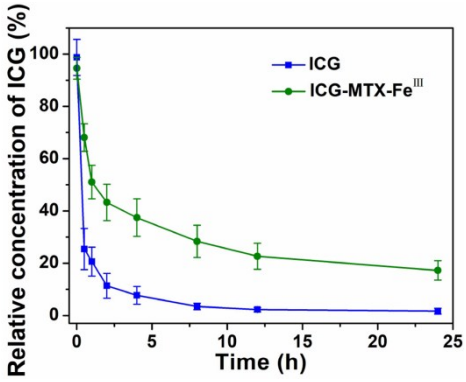

Fig. S23 Pharmacokinetic curves of ICG and ICG-MTX-Fe^{III}. Error bars represent mean ± SD (n = 4).

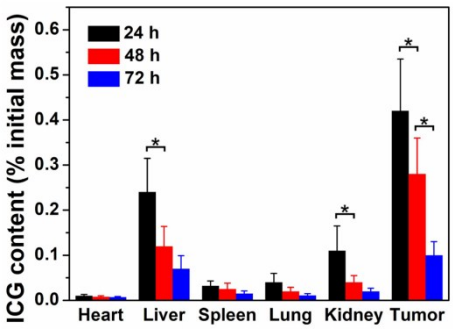

Fig. S24 The biodistribution of ICG-MTX-Fe$^{\text{III}}$ in main organs and tumors at different time intervals. Error bars represent mean ± SD (n = 4); *P < 0.05.

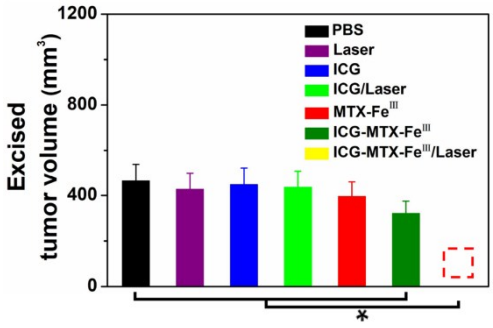

Fig. S25 Mean excised tumor volume of mice injected with PBS, ICG, MTX-Fe$^{\text{III}}$, and ICG-MTX-Fe$^{\text{III}}$ *via* caudal veins with/without laser irradiation on the last day. Error bars represent mean ± SD (n = 4); *P < 0.05.

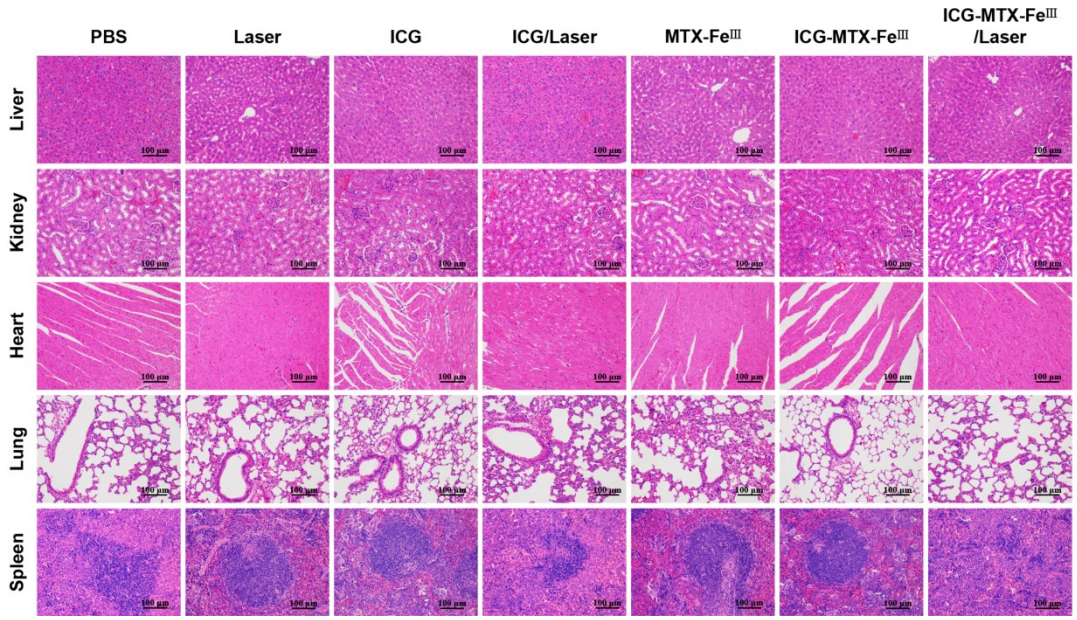

Fig. S26 Representative H&E-stained histological images obtained from normal tissues including liver, kidney, heart, lung, and spleen of HeLa tumor-bearing nude mice after different treatments.